

Excitons in linear carbon chains

Stella Kutrovskaia^{1,2,3*}, Anton Osipov^{3,4}, Stepan Baryshev⁵,
Anton Zasedatelev⁵, Alexey Povolotskiy⁶, Vlad Samyshkin³,
Olivia Pulci⁷, Davide Grassano⁷, Lorenzo Gontrani⁷, Richard
Hartmann⁸, Mikhail E. Portnoi^{9,10}, Alexey Kucherik^{1,2,3}, Pavlos
Lagoudakis^{5,11} and Alexey Kavokin^{1,2,11,12}

¹ School of Science, Westlake University, 18 Shilongshan Road, Hangzhou 310024, Zhejiang Province, China

² Institute of Natural Sciences, Westlake Institute for Advanced Study, 18 Shilongshan Road, Hangzhou 310024, Zhejiang Province, China

³ Department of Physics and Applied Mathematics, Stoletov Vladimir State University, 600000 Gorkii street, Vladimir, Russia

⁴ ILIT RAS — Branch of FSRC “Crystallography and Photonics” RAS, 1 Svyatoozerskaya, Shatura, 140700, Moscow region, Russia

⁵ Skolkovo Institute of Science and Technology, 30 Bolshoy Boulevard, bld. 1, 121205 Moscow, Russia

⁶ Institute of Chemistry, St. Petersburg State University, 198504, Ulianovskaya str. 5, St. Petersburg, Russia

⁷ Department of Physics, University of Rome Tor Vergata, Via della Ricerca Scientifica 1, I-00133 Rome, Italy

⁸ Physics Department, De La Salle University, 2401 Taft Avenue, 0922 Manila, Philippines

⁹ Physics and Astronomy, University of Exeter, Stocker Road, Exeter EX4 4QL, United Kingdom

¹⁰ ITMO University, St. Petersburg 197101, Russia

¹¹ Physics and Astronomy, University of Southampton, Highfield, Southampton, SO171BJ, United Kingdom

¹² Spin Optics Laboratory, St. Petersburg State University, 198504, Ulianovskaya str. 1, St. Petersburg, Russia

September 2019

E-mail: stella.kutrovskaia@westlake.edu.cn

Abstract. We synthesise and deposit on a substrate monoatomic chains of carbon atoms stabilised by gold nanoparticles. Resulting nano-objects are identified as polyynes: chains of carbon atoms linked by alternating single and triple electronic bonds. Raman, absorption and photoluminescence (PL) spectra reveal resonant features of straight polyne chains containing 10, 12, 14, 16 etc atoms, that is significantly beyond the theoretical stability limit of 6 atoms for free-standing carbon chains. Polyne is a direct band gap semiconductor whose lowest energy optical transition varies in the range between 2 and 5 eV depending on the number of atoms in the chain. Low temperature PL spectra reveal a characteristic triplet fine-structure that repeats itself for carbon chains of different lengths. The triplet is invariably

composed by a sharp intense peak accompanied by two broader satellites shifted by about 15 and 25 meV to the lower energy side of the main peak. We interpret these features as an edge-state neutral exciton, positively and negatively charged trions, respectively. The localization of exciton wave-functions at the end of gold-stabilised carbon chains is confirmed by ab-initio calculations. The time-resolved PL shows that the radiative life time of the observed quasiparticles is about 1 ns that is consistent with the characteristic exciton lifetimes in carbon nanotubes (CNT). The radiative lifetime increases with the increase of the length of the chain. At high temperatures a non-radiative exciton decay channel appears due to the thermal hopping of carriers between parallel carbon chains. In contrast to CNT excitons, the excitons in carbyne are characterised by lower binding energies (of the order of 15-20 meV), large oscillator strengths and extremely low inhomogeneous broadenings that allow for the detection of the fine structure of exciton and trion transitions. The observation of strong and narrow exciton resonances in PL spectra of monoatomic carbon chains paves the way to their applications in nano-lasers and single photon emitters.

Keywords: one-dimensional carbon chains, excitons, photoluminescence spectra, gold nanoparticles

1. Introduction

Several types of low-dimensional crystals based on carbon were attracting attention of the physical and chemical research communities in the XXI century. Nanodiamonds, fullerenes, carbon nanotubes and graphene demonstrate a variety of interesting and unusual electronic properties that make them promising for breath-taking applications in nano-electronics and photonics (1). One of the most challenging goals for the nanofabrication technology is the realization of ultimate one-dimensional crystals, monoatomic chains of carbon: the carbynes. Traces of two stable allotropes of carbyne (polyyne and cumulene) have been found in nature: in meteorite craters, interstellar dust, natural graphite and diamond mines (2; 3; 4). The high chemical reactivity of carbyne and its low stability at room temperature and atmospheric pressure makes it difficult to extract free standing carbon chains from natural sources. Moreover, multiple attempts to synthesize carbyne artificially yielded modest or no success so far (5). Until now, to the best of our knowledge, stable freestanding samples of straight carbon chains have not yet been realised. Their synthesis appears to be a formidable challenge as, in general, infinite one-dimensional atomic chains are unstable in vacuum. According to the Landau theorem (6), fluctuations prevent the formation of ideal one-dimensional crystals. Therefore, many works have been devoted to the artificial stabilization of carbyne. The stabilization may be achieved by the use of heavy anchor atomic groups (7), the confinement of carbon chains in double-wall carbon nanotubes (8), or their pinning to metal surfaces (9). The synthesis of free-standing carbon chains remains one of the Holy Grails of nanophysics and nanochemistry. If realized experimentally, these one-dimensional crystals would exhibit unique mechanical, optical and electronic properties (10). According to the recent theoretical works (11), carbyne would be the

most robust of all known crystals. It may take one of two allotropic forms: the cumulene, where neighboring carbon atoms are linked with double electronic bonds, and polyynes, where single and triple electronic bonds alternate (see the schematic in Figure 1(a)). In polyynes, the interatomic distances are predicted to be 0.133 nm (C-C) and 0.122 nm (C = C) which yields the lattice constant of 0.255 nm. These interatomic separations are significantly less than those in graphite where the spacing between neighbouring atoms is of 0.142 nm, while the spacing between atomic planes is 0.335 nm. This is why the predicted Young modulus of carbyne is somewhat higher than in graphene and one order of magnitude higher than that of diamond (12). The electrical conductivity and magnetic properties of carbyne can be dramatically varied by stretching and twisting the atomic chains (13). The strain induced switching of conductivity in carbyne has been observed recently (14). Isolated monoatomic chains are predicted to demonstrate peculiar spin-dependent quantum transport effects (15). Carbynes are also expected to exhibit superconductivity at high temperatures (16). Ab-initio calculations (11) show that polyynes are direct band gap semiconductors with the band gap achieving 2.58 eV gap for polyynes. Our own ab-initio calculations of the band structure of stabilised infinite polyyne chains predict the existence of a direct electronic band-gap of 2.7 eV at the edge of the Brillouin zone (see Figure 1(b)). Being direct-gap semiconductors, carbynes are expected to possess unusual optical properties. In particular, their nonlinear optical response is expected to be giant (17). Indeed, unlike graphite or graphene which are strong absorbers and do not emit light, and carbon nanotubes where the multivalley band structure leads to dark excitons suppressing the luminescence, carbyne is often called “white carbon” because of its ability to emit visible light. The band gap of finite size linear chains dramatically depends on the number of carbon atoms in a chain, being the larger the shorter the chain. In the following we shall focus on straight polyyne chains containing from 8 to 24 carbon atoms whose band structure is reduced to a sequence of discrete energy levels similar to molecular orbitals. The gap between the highest occupied molecular orbital (HOMO) and the lowest unoccupied molecular orbital (LUMO) varies in the range of 3-5 eV (see the schematic in Figure 1(d)). This results in a large spectral distribution of allowed optical transitions in such systems.

In this paper, we study stable elongated carbon chains synthesised by the laser ablation technique in a colloidal solution. The mechanical stabilisation of carbyne is achieved due to the electron bonding of carbon chains to gold nanoparticles (NPs). We obtain the polyyne allotropic form of carbyne, which is characterised by specific discrete vibron modes clearly seen in the Raman spectra of the solution. When deposited on a substrate, the stabilized chains demonstrate straight parts whose lengths significantly exceed the theoretical limit for a free stable monoatomic carbon chain. The high-resolution transmission electron microscopy (HR TEM) of our samples shows straight linear carbon chains of the lengths that sometimes exceed 5 nm. Most interestingly, at the liquid Helium temperature, a pronounced fine structure emerges in the photoluminescence (PL) spectra of deposited carbyne on the top of broad resonances corresponding to polyyne chains of different lengths. This fine structure

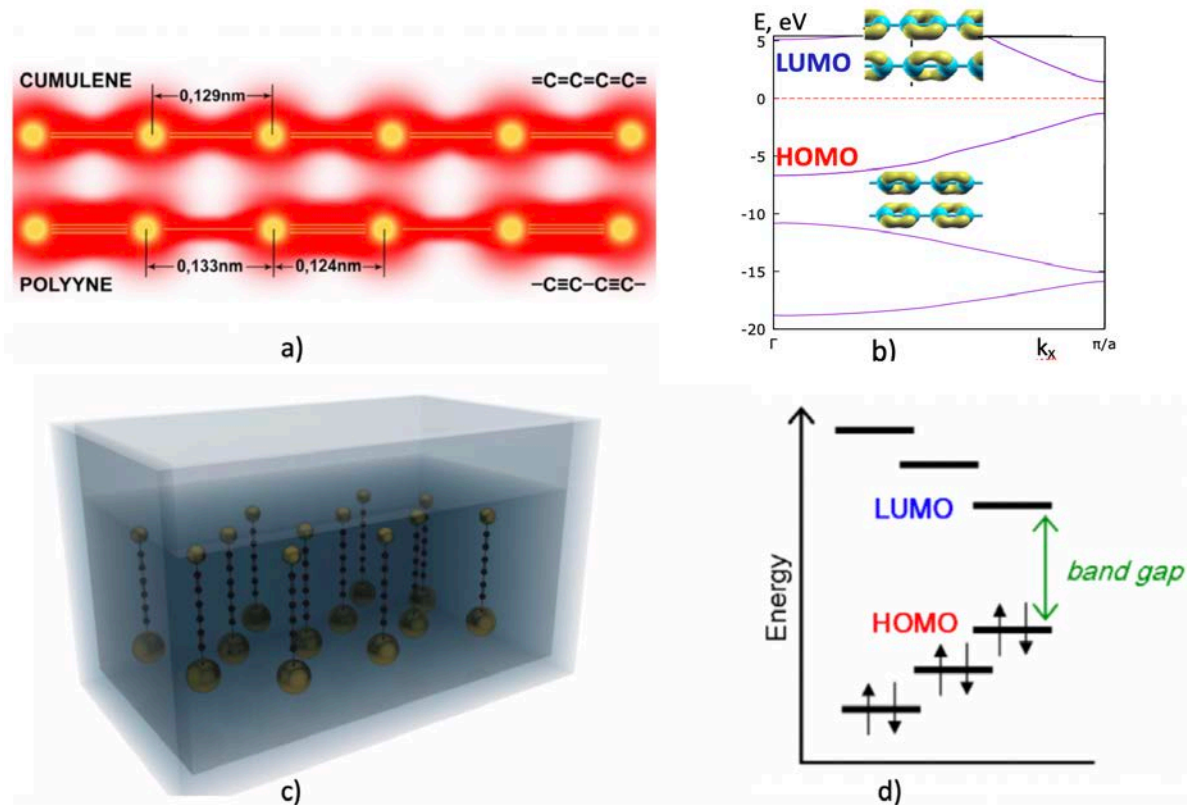


Figure 1: The structure of carbynes: (a) the schematic distribution of the electron density in cumulene and polyynes allotropes of carbyne. (b) shows the band structure of an infinite polyyn chain predicted by our ab-initio calculation, and the HOMO, LUMO doubly degenerate orbitals. (c) illustrates the concept of stabilisation of monoatomic carbon chains by gold nanoparticles in a solution. (d) shows schematically the energy level structure of a finite polyyn chain with two gold nanoparticles attached to its ends.

is composed invariably by a high amplitude narrow peak accompanied by two lower energy satellites which can be attributed to the exciton resonance and two trion resonances, respectively. The time-resolved photoluminescence (TRPL) spectra show that the radiative life-time of the observed transitions is of the order of 1 ns, that is similar to the data reported for excitons in CNTs (18). At high temperatures, the double exponential decay of the PL signal is observed with a fast exponential characterising the thermal dissociation of excitons, and the slow exponential corresponding to their radiative decay. The exciton radiative lifetime decreases with the decrease of the length of the chain. We refer to the Su-Schrieffer-Heeger model (19) to argue that the transition that dominates low temperature PL spectra is based on the edge electronic states that form the HOMO- LUMO pair in carbon chains stabilised by gold NPs. This interpretation is confirmed by the ab-initio calculation.

2. The synthesis of monoatomic carbon chains

We employ the method of synthesis of the carbon chains based on the laser ablation of a carbon target in liquid (20). The procedure is schematically illustrated in Figure 1 (c). The stabilization of the linear carbon chains is achieved by adding spherical gold NPs to the solution. NPs having average sizes of either 10 or 100 nm attach themselves to the ends of carbon chains. If NPs at the opposite ends are of different sizes, the difference of their work functions results in the charging of the carbon-NP complex that acquires a stationary dipole moment. This dipole polarization provides a tool for the chain manipulation by an applied voltage. The laser processing described above leads to the formation of polyynes threads. The presence of polyynes in the studied solution is confirmed by the two pronounced maxima in its Raman spectrum shown in Fig. 2(a). The peak at 1050cm^{-1} corresponds to a single carbon bond (C-C) whereas the peak at 2175 cm^{-1} corresponds to the triple bond (C = C) (27). The broadening of the single carbon bond peak is explained by the fact that this bond is weaker than the other one, which is why it is subject to the Peierls distortion (28). This is confirmed by the presence of a local maximum of the Raman signal in the vicinity of 800 cm^{-1} , which is due to the mechanical stress in the chain (29). Also, one can observe the frequency shift corresponding to the formation of the gold-carbon bond, which is believed to be longer and weaker than the normal covalent C-C bond (9).

The absorption spectrum of the obtained solution (see Fig. 2(b)) demonstrates a pronounced band in the wavelength range of 240-350 nm which is typical for short carbon chains. One can see that the highest magnitude of absorption is detected in the spectral vicinity of 243 nm. In the inset to Fig. 2(b) the experimental spectrum is decomposed in several absorption contributions taken from the *ab initio* calculation for the chains of varying length. Our calculations are in a good agreement with (30). The small deviation between the central frequency positions of the observed peaks and our calculation results is caused by the polyynes stabilization by gold NPs in our experiments. Figure 2(c) shows the absorption magnitude distribution of the synthesised carbon chains extracted from the fit of the absorption spectrum shown in the inset to the right panel of Figure 2(b). One can see that the chains of the lengths between 10 and 26 atoms are present in the solution. Remarkably, only carbon chains with even numbers of atoms contribute to the absorption spectra. We attribute this parity selection rule to the impact of gold NPs: at the edges, carbon atoms are always linked by single electron bonds to the metal surface, which is why the number of carbon atoms in polyynes chains having both their ends attached to metal is necessarily even.

3. Deposition and alignment of stabilised polyynes chains

The alignment of synthesised carbon chains deposited on a surface is essential, as chaotic criss-crossing of carbynes may result in the degradation of their electronic and optical properties. In order to avoid this effect, we intentionally order the carbon chains by

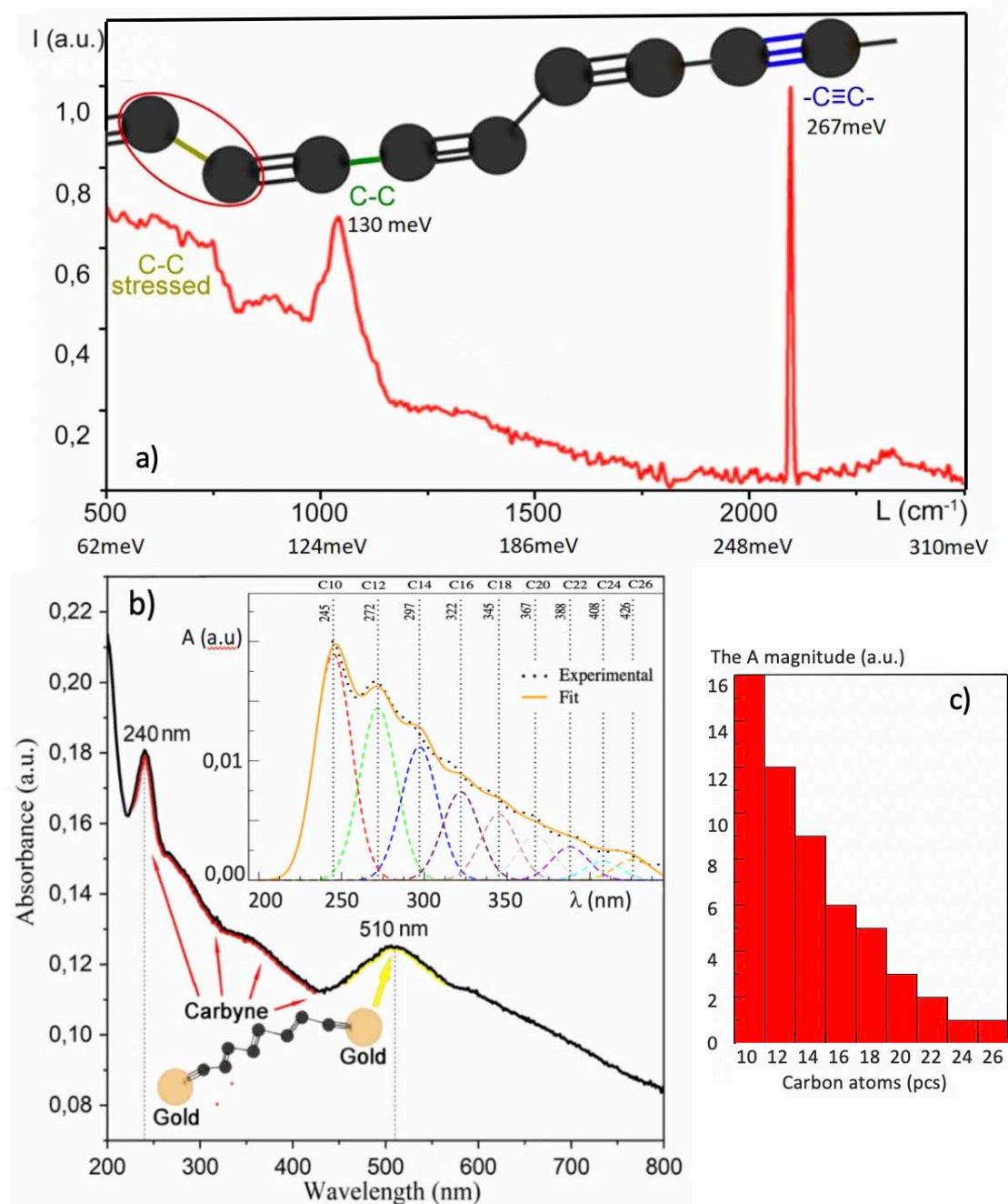


Figure 2: Optical investigation of carbyne chains in a colloidal solution: (a) the Raman spectra of the solution containing linear carbon chains stabilised by gold NPs. The peaks correspond to characteristic vibron modes of the polyyne allotrope. (b) the absorption spectrum (A (a.u.)) of the solution containing gold-stabilised carbon chains. The inset shows the decomposition of the experimental spectrum into a sequence of calculated absorption peaks corresponding to the polyynes chains of different lengths. (c) shows the absorption magnitude (marked as the A magnitude) distribution in straight polyynes chains extracted from the fit of the absorption spectra.

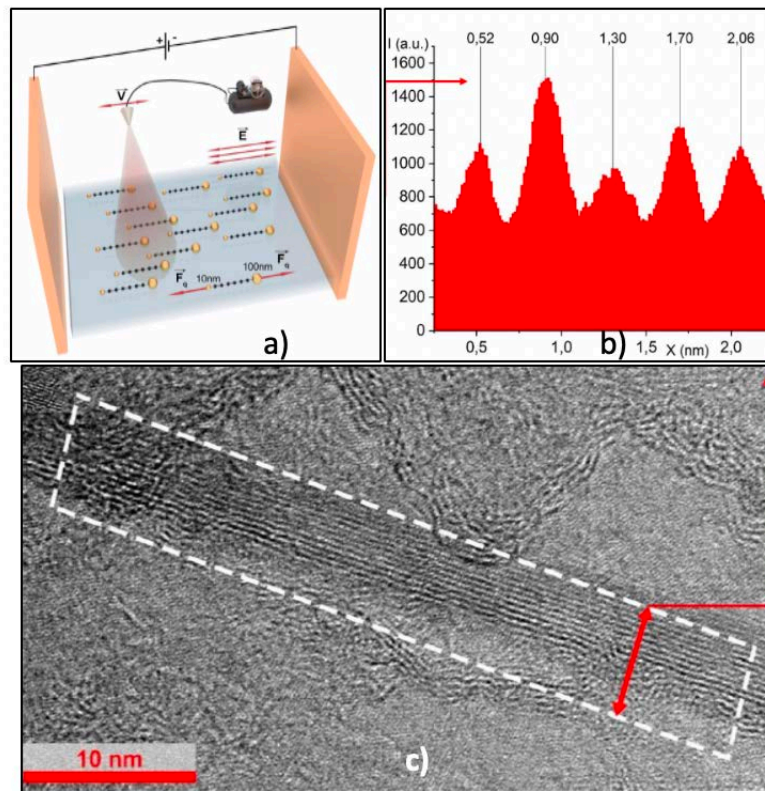


Figure 3: Deposition and characterisation of carbon chains: (a) illustrates the applied method of deposition of the aligned carbon chains stabilised by gold NPs of different sizes. Due to the difference in work functions of gold nanoparticles attached to the ends of the chain, it becomes dipole polarised. The external electric field orients the polarised chains, so that their majority appears to be aligned when deposited on a substrate by sputtering, (b) shows the HR TEM profile of this structure measured in the direction perpendicular to the chains. The profile is taken along the red arrow in the HR TEM image shown in (c).

passing the solution through the stationary electric field in the course of sputtering (see the scheme in Figure 3(a)). As a result, we were able to deposit long parallel chains of carbyne. A spectacular example of the chains exceeding the length of 40 nm is seen in the HR TEM image (Figure 3(c)). Interestingly, the ensemble of carbon chains forms a kind of one-dimensional Van-der-Waals crystal, where the distance between neighbouring chains exceeds the interatomic distance in a single chain by a factor of 3, approximately (see Figure 3(b)).

4. Low-temperature PL spectra of deposited carbynes

In the PL experiments, we excited the deposited carbynes quasi-resonantly, at the wavelengths between 370 and 390 nm. The strong emission at the wavelengths over 400 nm has been detected. As there were necessarily thousands of individual carbon

chains under our pump spot, which is of 2 size, the PL signal is always built from contributions of carbon chains of different lengths. The chains containing from 8 to 18 atoms (24) typically dominate the spectra. Figure 4(a) shows the characteristic PL spectra featuring broad resonances corresponding to the chains of different lengths emitting in the spectral range from 2.4 to 3.0 eV. The lowest energy optical transition shifts to the red with the increase of the length of the chain, in full agreement with the theoretical predictions (24). As the temperature goes down to 4K, a very distinct and peculiar fine structure emerges on the top of each broad PL peak (Figure 4(b)). Nearly identical triplet structures are observed for the chains of 10, 12, 14, 16 atoms. A strong and very narrow peak with a full width at half maximum (FWHM) of only 3-4 meV has two broader and lower satellites shifted by about 15 and 25 meV towards lower energies. This observation is in a stark contrast with the exciton spectra of carbon nanotubes (18) that typically feature strongly inhomogeneously broadened peaks with typical FWHM of several tens meV. The left panel of Figure 5 shows the time-resolved photoluminescence (TRPL) data acquired at the high temperature (Figure 5(a)) and liquid Helium temperature (Figure 5(c)). The TRPL is spectrally resolved, the selected bands being indicated in the insets. The high temperature spectra show the double-exponential behaviour reflecting the interplay between non-radiative (thermal hopping) and radiative channels of the exciton decay. The extracted decay times are plotted in Figure 5(b). The low temperature spectra show the monoexponential decay of the excitonic photoluminescence with a characteristic decay time of the order of 1 ns that is comparable with the typical radiative life times of excitons in carbon nanotubes (33). The exciton radiative life-time increases with the increase of the length of the chain following the anticipated behaviour of the matrix element of the dipole transition.

5. Discussion

The triplet structures emerging as the temperature decreases are indicative of excitonic transitions. The exciton binding energy may be defined as the difference of the transition energies between an electron and a hole belonging to the same carbon chain and between an electron and a hole located in different carbon chains. The exciton dissociation into a radiatively inactive electron-hole pair by thermal hopping of one of the carriers to the neighboring chains (Figure 3 (c)) is expected to govern the temperature dependence of the intensity of the observed excitonic peaks. From the temperature resolved PL spectra we estimate the exciton binding energy to be of the order of 15-20 meV. Note that the excitons are expected to be localised at the ends of the carbon chains forming an equivalent of Su-Schrieffer-Heeger states (19) as confirmed by the results of our ab-initial calculation shown in Figure 6(e,f,g). The exciton binding energy is governed by the exchange term, that is expected to be of the order of 10-20 meV in agreement with the PL data. Note, that the electron-hole exchange interaction is only important if both carriers are located in the same carbon chain. Once one of the carriers migrates to a parallel chain, the electron-hole overlap strongly decreases, and the exchange contribution to

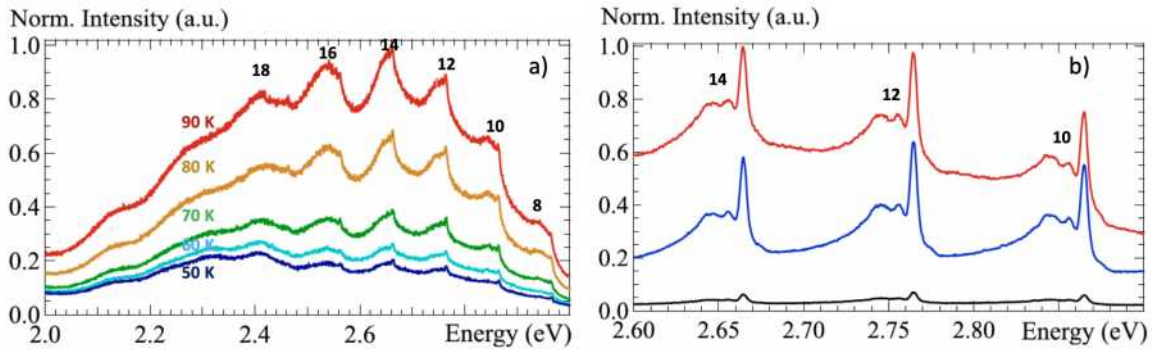


Figure 4: PL spectra of the deposited polyynes chains of different lengths (the number of atoms in the chain is indicated on the top of the corresponding spectral resonance): (a) shows the spectra taken at temperatures from 90 to 50K (red curve corresponds to 90 K, yellow curve corresponds to 80K, green curve corresponds to 70K, teal curve corresponds to 60K, blue curve corresponds to 50K). The laser excitation wavelength is 390 nm with the intensity of 5 mW and the acquisition time of 10 s. (b) shows the PL spectra taken at 4K. Red, blue and black curves correspond to the excitation wavelengths of 390, 380 and 370 nm, respectively. The acquisition time is 40 s.

the exciton energy is lost. Two lower energy satellites clearly visible in the excitonic spectra of the carbon chains containing 10, 12 and 14 atoms may be associated to zero-phonon lines (31), phonon replicas, bi-excitons or charged excitons, in principle. We rule out the three first scenario as (i) the measured vibron energies in polyynes are of 130 and 267 meV (Figure 2(a)) that strongly exceeds the observed splittings between the main peak and satellite peaks (15-25 meV), (ii) the typical optical phonon energy in polyynes is expected to be of the order of 100 meV (32) that is also significantly larger than the observed splittings, and (iii) the bi-exciton line intensity would vanish at low excitation powers, that contradicts our data. Charged exciton complexes (trions) are likely to be formed in our system due to the vicinity of metal nanoparticles that can supply carbon chains with extra charge carriers, see the schemes in Figure 6 (b,c). The dipole polarisation of gold-stabilised carbon chains is confirmed by their alignment in the external electric field (see the scheme in Figure 3(a)), thus the presence of extracharges localised at the ends of some of the chains is beyond any doubts. The oscillator strengths of negatively charged (X^-) and positively charged (X^+) trion transitions are expected to be roughly twice lower than the oscillator strength of the exciton transition as the spin degeneracy is lifted in the presence of an extra electron (hole), that is also consistent with the data (see Figure 6(d)).

Figure 6 (e,f,g) presents the plots of HOMO and LUMO wavefunctions and of the total electron density of Au-stabilised carbon chains, obtained from *in vacuo* DFT calculations with localised basis sets, are shown for the polyynes chain of 14 carbon atoms capped with two Au₁₃ nanoparticles. Indeed, in the calculated distributions of the HOMO and the total density (top and bottom panel) it appears that most part of the

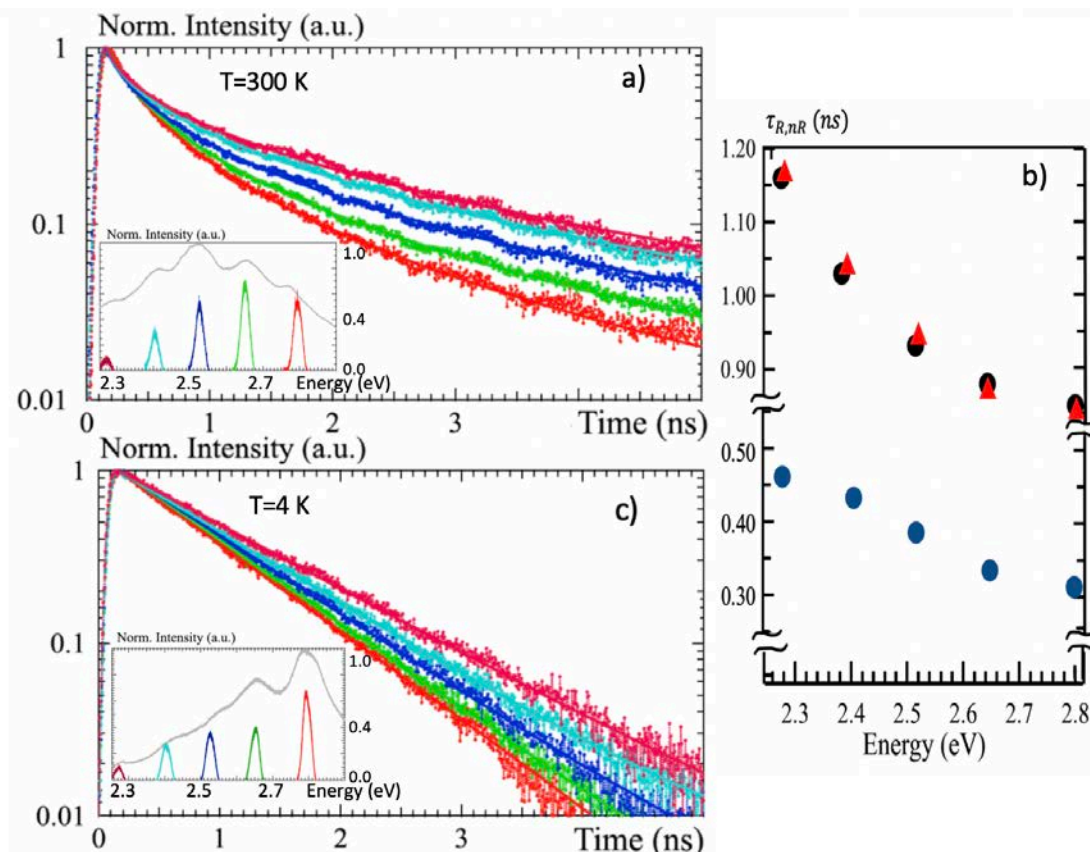


Figure 5: The time-resolved photoluminescence data: (a) and (c) show the TRPL data acquired at the room temperature and at 4K, respectively. The insets show the spectral bands that correspond to the TRPL curves of (a,c), respectively. The colors match.(b) shows the extracted decay times of the TRPL signal taken at room temperature and Helium temperature, respectively. Red and black points correspond to the deduced radiative decay time at the room temperature (red) and Helium temperature (black). The blue points show the non-radiative decay times, extracted from the room temperature TRPL curves (a).

electron cloud is located around gold atoms and partially on the shorter C-C bonds of the polyyne moiety. Excitons and trions based on HOMO-LUMO transitions are localised at the ends of the atomic chains. This strong spatial localisation and significant electron-hole overlap are responsible for a large oscillator strength of the corresponding optical transitions. The similar plots obtained for C14 without gold terminations (see Figure S1 and S2 of the Supplemental Material) lack these features, and the electronic density tends to vanish moving from the centre to the ends of the chain. We conclude that gold-stabilized carbon chains are highly advantageous for the observation of excitonic effects as they provide a very strong spatial localisation, large oscillator strength and low inhomogeneous broadening of the exciton and trion transitions.

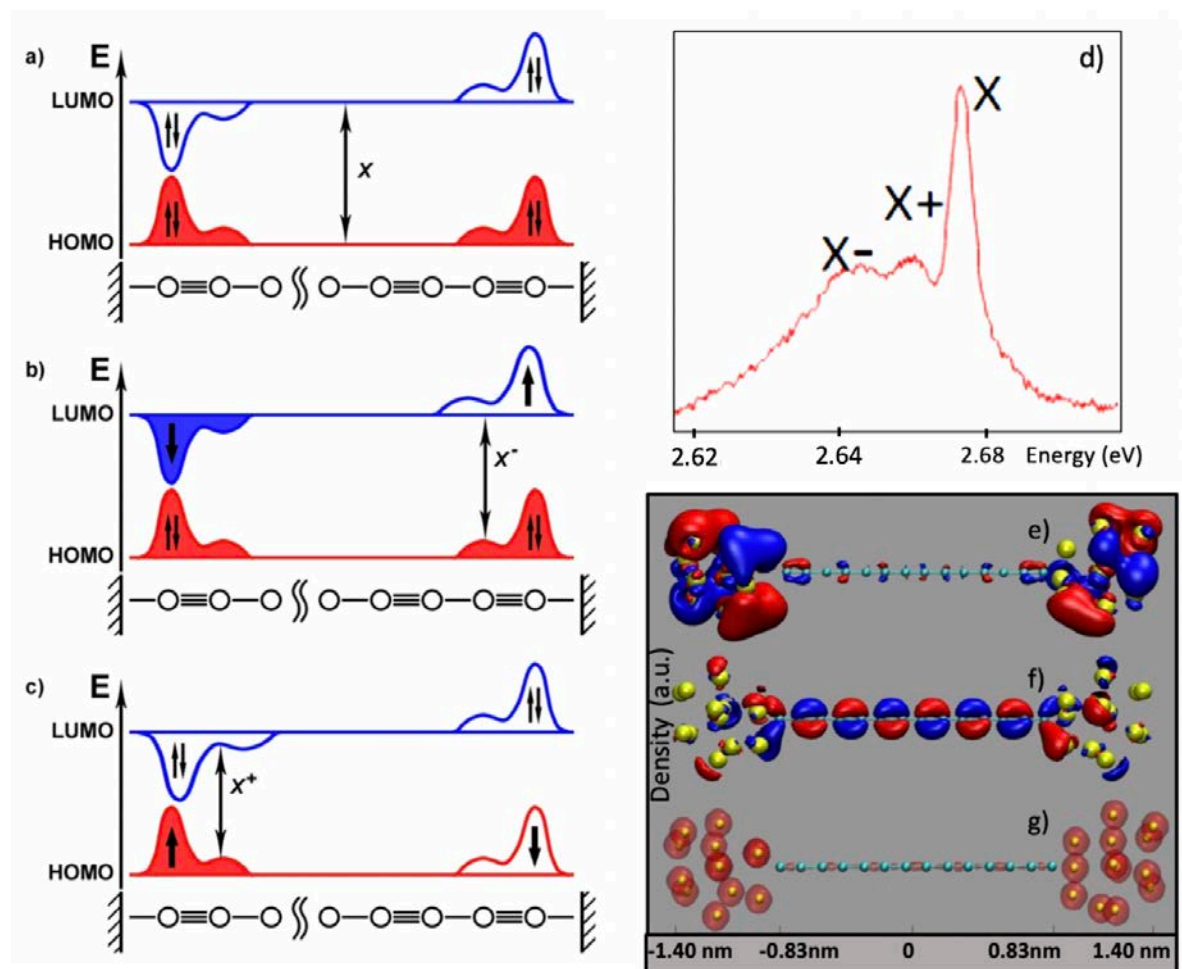


Figure 6: The scheme of excitonic transitions in a monoatomic polyyn chain. (a) The neutral exciton (X) is formed by even and odd edge states that originate from the HOMO-LUMO pair. (b,c) The trion transitions in charged chains, where the left-right symmetry is broken so that the optical transition occurs between either the original HOMO state and the spin polarised electron state localised at one of the edges (X^-) or between the hole state localised at one of the edges and the original LUMO state (X^+). (d) The enlarged PL spectrum of a characteristic triplet corresponding to the 14- atom chain that shows the relative oscillator strengths of exciton and trion transitions. Molecular orbitals and total electron density plots for a model system containing a polyyn chain composed of 14 carbon atoms capped with two gold nanoparticles ($C_{14}-Au_{132}$) for HOMO (e), LUMO (f). The total calculated electron density (g). Red and blue lobes correspond to positive and negative values, respectively.

6. Summary

The sharp peaks emerging at low temperatures in the PL spectra of gold-stabilised carbon chains are indicative of the exciton and trion transitions based on the edge electronic states

in the chains. The triplet fine structure that is very well seen at Helium temperature is essentially independent of the length of the chain, while the absolute energies of the transitions become larger for the shorter chains. This observation demonstrates a high potentiality of synthesised polyynes chains for optoelectronic applications, especially in nano-lasing and single photon emitters. Moreover, the observation of radiatively active excitons in ultimate one-dimensional crystals, carbynes, is of a great fundamental interest. Further studies are needed to fully reveal properties of excitons and trions in carbynes.

7. Methods

We study the photoluminescence (PL) of carbyne chains using the 140 fs pulsed 80 MHz repetition rate Ti: Sapphire laser system (Coherent Cameleon Ultra II) coupled to an optical parametric oscillator allowing for fine control over the excitation energies. As the sample is mounted in a closed-cycle cryostat Montana Instruments Cryostat C2 we carry out PL measurements in a vacuum within the temperature range of 4K- 300K. The optical excitation we employ in these experiments is tightly focused onto a sample by Mitutoyo M Plan APO SL x50 microscope objective with a numerical aperture of 0.42. Note that we use three different excitation wavelengths to elucidate the nature of the observed fine lines in the PL spectra, namely 390, 380 and 370 nm as shown in Figure 4. We collect PL signal in the transmission configuration using the same Mitutoyo M Plan APO SL x50 microscope objective. To avoid any parasitic signal in PL spectra we filter out optical excitation with a short pass filter cutting light above 561nm, and in the collection path we use a long pass filter transmitting light above 400nm to get rid of the optical excitation signal. Being properly filtered, the PL from the sample is coupled into a 750 mm focal length spectrometer (Princeton Instruments SP2750) equipped with a charge-coupled device camera (Pixis-XB: 1024BR) with 1024x1024 imaging array. In all the spectroscopic measurements we use 1200 grooves mm^{-1} grating and 20 μm entrance slit, as well as step and glue technique to record the entire PL spectra represented in Figures 4 and 5. The spectral resolution of our setup is 100 pm. Despite omnipresent background emission from the substrate (above 650 nm) we systematically observe several distinct peaks in the PL of the sample that correspond to the optical transitions of carbyne chains of the different lengths. We further extend our spectroscopic analysis with in-depth study of the PL dynamics attributed to the identified optical transitions. We employ a standard time-correlated single-photon counting technique (TCSPC), with detection wavelengths scanned across the full emission bandwidth using a variable birefringent filter device (Liquid crystal tunable filter Varispec). The recorded spectra of the PL coupled to TCSPC system are shown in Figure 4(a) and (b). We extract spectral lines within 5 nm linewidth that corresponds to the exciton and trion transitions. We use a single-photon avalanche photodiode (APD) (id100-MMF50) together with TCSPC module (SPC-160, Becker & Hickel GMBH) to detect photon events related to the PL. The typical count rate is 10^3 - 10^4 counts/s while a dark count rate is 40 Hz. The APD response

defines the time resolution in our system, which is as short as 60 ps. By using the aforementioned technique, we measure emission decay for five individual optical transitions (Figure 5 (a,b,c,d)).

The Density Functional Theory calculations for the infinite chain were performed using the QUANTUM ESPRESSO package (34). We tested several exchange and correlation potentials: LDA, LSDA, PBE, PBE0, HSE06. An energy cutoff of 90 Ry and a k-points mesh of 16x1x1 k-points was used to optimize the atomic positions. A supercell with a vacuum of about 30 Å was employed, in order to avoid spurious interactions between neighbouring chains. We found that the polyyne geometry (that is, an infinite chain with single and triple bonds) can only be obtained with the use of hybrid pseudopotentials. In LDA, LSDA or PBE, instead, cumulene is the only stable structure, with a zero electronic gap. Optical spectra for varying lengths of the carbon chains (from 10 up to 26 C atoms) were obtained within Time Dependent Functional Theory (TDDFT) calculations with PBE0 kernel, using the code Gaussian (35) with triple-zeta 6-311+G(d,p) basis set plus LANL2DZ pseudopotential for gold core electrons (36), after geometry optimisation. In all the considered cases, polyyne configurations have a lower energy than cumulene.

Acknowledgments

The work of S.K. and A.KA. is supported by the Westlake University (Project No. 041020100118). P.L. and A.KA. acknowledge the UK's Engineering and Physical Sciences Research Council (grant EP/M025330/1 on Hybrid Polaritonics). This work was also partially supported by RFBR grants 17-32-50171, 18-32-20006 and 19-3290085. A.KA. acknowledges Saint-Petersburg State University for the research grant ID 40847559. The financial support from the EU MSCA RISE project CoExAN (GA 644076) is acknowledged. L.G. acknowledges support from Regione Lazio, through Progetto di Ricerca 85-2017-15125 according to L. R. 13/08. CPU computing time was granted by CINECA HPC center and by the "Departments of Excellence-2018" Program (Dipartimenti di Eccellenza) of the Italian Ministry of Research, DIBAF-Department of University of Tuscia, Project "Landscape 4.0 - food, wellbeing and environment" (Prof. Nico Sanna). The synthesis and deposition of carbynes have been performed at the Vladimir State University. Raman spectra and absorbance were measured at the Center for Optical and Laser Materials Research, Research Park, St. Petersburg State University. TEM measurements have been performed in the "System for microscopy and analysis" LLC, Moscow.

Author Contributions

S.K. has conceived the work and analysed experimental data;

A.O. contributed to the laser ablation experiments;

S.B. performed the PL experiments;

A.Z. analyzed the PL data;
A.P. performed optical absorption and Raman measurements;
V.S. realized the carbyne deposition on a substrate;
O. P. contributed to the ab-initio model and revised the manuscript;
D.G. performed the ab-initio calculation for an infinite chain;
L. G. performed the ab-initio calculation for finite chains;
R. H. contributed to the fit of the PL spectra;
M. E.P. contributed to the theoretical model and interpretation of the results;
A.K. contributed to the synthesis of monoatomic carbon chains and realized HR TEM microscopy study;
P. L. contributed to the measurements and interpretation of the PL and time-resolved PL spectra;
A.KA. contributed to the interpretation of the results and has coordinated the collaborative work;
S. K. and A.KA. have written the manuscript.

Competing Interests statement

Conflict of interest: None declared

Ethical approval: Not required

References

- [1] Y. Segawa, H. Ito, and K. Itami, Structurally uniform and atomically precise carbon nanostructures, *Nature Reviews Materials* **1** (2016).
- [2] A. E. Goresyand and G. Donnay, A new allotropic form of carbon from the ries crater, *Science* **161**, 363364 (1968).
- [3] A. Whittaker, Carbon: Occurrence of carbyne forms of carbon in natural graphite, *Carbon* **17**, 2124 (1979).
- [4] X.-Y. Chuan, Z. Zheng, and J. Chen, Flakes of natural carbyne in a diamond mine, *Carbon* **41**, 18771880 (2003).
- [5] H. Kroto, Carbyne and other myths about carbon, *Chemistry World* **7** (2010).
- [6] L. Landauand and E. Lifshitz, *Statistical physics, part 1: Volume 5 (course of theoretical physics, volume 5)*, Publisher: Butterworth-Heinemann **3** (1980).
- [7] T. Gibtner, F. Hampel, J.-P. Gisselbrecht, and A. Hirsch, End-cap stabilized oligoynes: Model compounds for the linear sp carbon allotrope carbyne, *Chemistry - A European Journal* **8**, 408432 (2002).
- [8] L. Shi *et al* , Conned linear carbon chains as a route to bulk carbyne, *Nature Materials* **15**, 634639 (2016).
- [9] A. Rabia, F. Tumino, A. Milani, V. Russo, A. Li Bassi, S. Achilli, G. Fratesi, G. Onida, N. Manini, Q. Sun. W. Hu, and C.S. Casari, *Scanning tunneling microscopy*

- and Raman spectroscopy of polymeric sp-sp² carbon atomic wires synthesized on the Au(111) surface, *Nanoscale*, DOI: 10.1039/c9nr06552k (2019).
- [10] R. Khanna, M. Ikram-Ul-Haq, A. Rawal, R. Rajarao, V. Sahajwalla, R. Cayumil, and P. S. Mukherjee, Formation of carbyne-like materials during low temperature pyrolysis of lignocellulosic biomass: A natural resource of linear sp carbons, *Scientific Reports* 7, 10.1038/s41598-017-17240-1 (2017).
- [11] M. Liu, V. I. Artyukhov, H. Lee, F. Xu, and B. I. Yakobson, Carbyne from first-principles: Chain of c atoms, a nanorod or a nanorope, *ACS Nano* 7, 100175 (2013).
- [12] L. Itzhaki, E. Altus, H. Basch, and S. Hoz, Harder than diamond: Determining the crosssectional area and Youngs modulus of molecular rods, *Angewandte Chemie International Edition* 44, 74327435 (2005).
- [13] O. Cretu, A. Botello-Mendez, I. Janowska, C. Pham-Huu, J.-C. Charlier, and F. Banhart, Electrical transport measured in atomic carbon chains, *Nano Letters* 13 (2013).
- [14] A. L. Torre, A. Botello-Mendez, W. Baaziz, J. C. Charlier, and F. Banhart, Strain-induced metalsemiconductor transition observed in atomic carbon chains, *Nature Communications* 6 (2015).
- [15] Z. Zanolli, G. Onida, and J.-C. Charlier, Quantum spin transport in carbon chains, *ACS Nano* 4, 5174 (2010).
- [16] Z. K. Tang, L. Zhang, N. Wang, X. X. Zhang, G. H. Wen, G. D. Li, J. N. Wang, C. T. Chan, and P. Sheng, Superconductivity in 4 angstrom single-walled carbon nanotubes, *Science* 292, 24622465 (2001).
- [17] C. R. Ma, J. Xiao, and G. W. Yang, Giant nonlinear optical responses of carbyne, *J. Mater. Chem. C* 4, 4692 (2016).
- [18] Jonah Shaver and Junichiro Kono, Temperature-dependent magnetophotoluminescence spectroscopy of carbon nanotubes: evidence for dark excitons, *Laser & Photon. Rev.* 1, No. 3, 260-274 (2007).
- [19] W. P. Su, J. R. Schrieffer, and A. J. Heeger, Solitons in polyacetylene, *Phys. Rev. Lett.* 42, 1698 (1979).
- [20] A. O. Kucherik, S. M. Arakelian, S. V. Garnov, S. V. Kutrovskaia, D. S. Nogtev, A. V. Osipov, and K. S. Khor'kov, Two-stage laser-induced synthesis of linear carbon chains, *Quantum Electronics* 46, 627 (2016).
- [21] N. Rozhkova, S. Rozhkov, and A. Goryunov, Natural graphene-based shungite nanocarbon, *Carbon Nanomaterials Sourcebook* , 153176 (2016).
- [22] H. Tammet, U. Horrak, and M. Kulmala, Negatively charged nanoparticles produced by splashing of water, *Atmospheric Chemistry and Physics* 9, 357367 (2009).
- [23] G. Yang and C. X. Wang, Laser ablation in liquids: principles and applications in the preparation of nanomaterials, Ch. 3 (CRC Press, 2012).

- [24] B. Pan, J. Xiao, J. Li, P. Liu, C. Wang, and G. Yang, Carbyne with finite length: The one-dimensional sp carbon, *Science Advances* 1, 10.1126/sciadv.1500857 (2015).
- [25] O. V. Yazyev and A. Pasquarello, Effect of metal elements in catalytic growth of carbon nanotubes, *Physical Review Letters* 100, 156102 (2008).
- [26] A. Kucherik, S. Arakelian, T. Vartanyan, S. Kutrovskaya, A. Osipov, A. Povolotskaya, A. Povolotskii, and A. Man'shina, Laser-induced synthesis of metalcarbon materials for implementing surface-enhanced raman scattering, *Optics and Spectroscopy* 121, 263270 (2016).
- [27] R. B. Heimann, S. E. Evsyukov, and L. Kavan, Carbyne and carbynoid structures, Vol. 21 (Springer Science & Business Media, 1999).
- [28] R. Peierls, Transition temperatures, *Helvetica Physica Acta.* 2, 7 (1934).
- [29] E. A. Buntov, A. F. Zatsypin, M. B. Guseva, and Y. S. Ponomov, 2d-ordered kinked carbyne chains: Dft modeling and raman characterization, *Carbon* 117, 271278 (2017).
- [30] F. Cataldo, Synthesis of polyynes in a submerged electric arc in organic solvents, *Carbon* 42, 129142 (2004).
- [31] P. Tamarat, A. Maali, B. Lounis, and M. Orrit, Probing the spectral dynamics of single terrylenediimide molecules in low-temperature solids, *J. Phys. Chem. A* 104, p. 1 (2000).
- [32] E. Montaani, Quasiparticles and excitonic gaps of one-dimensional carbon Chains, *Phys.Chem.Chem.Phys.*,18, 14810 (2016).
- [33] A.R. Amori, Zh. Hou, T.D. Krauss, Excitons in Single-Walled Carbon Nanotubes and Their Dynamic, *Annu. Rev. Phys. Chem.* 69:81-99 (2018).
- [34] P. Giannozzi, S. Baroni, N. Bonini, M. Calandra, R. Car, C. Cavazzoni, D. Ceresoli, G. L. Chiarotti, M. Cococcioni, I. Dabo, et al. *Journal of physics: Condensed matter* 21, 395502 (2009); P. Giannozzi, O. Andreussi, T. Brumme, O. Bunau, M. B. Nardelli, M. Calandra, R. Car, C. Cavazzoni, D. Ceresoli, M. Cococcioni, et al., *Journal of Physics: Condensed Matter* 29, 465901 (2017).
- [35] M. J. Frisch, G. W. Trucks, H. B. Schlegel, G. E. Scuseria, M. A. Robb, J. R. Cheeseman, G. Scalmani, V. Barone, G. A. Petersson, H. Nakatsuji, X. Li, M. Caricato, A. V. Marenich, J. Bloino, B. G. Janesko, R. Gomperts, B. Mennucci, H. P. Hratchian, J. V. Ortiz, A. F. Izmaylov, J. L. Sonnenberg, D. Williams-Young, F. Ding, F. Lipparini, F. Egidi, J. Goings, B. Peng, A. Petrone, T. Henderson, D. Ranasinghe, V. G. Zakrzewski, J. Gao, N. Rega, G. Zheng, W. Liang, M. Hada, M. Ehara, K. Toyota, R. Fukuda, J. Hasegawa, M. Ishida, T. Nakajima, Y. Honda, O. Kitao, H. Nakai, T. Vreven, K. Throssell, J. A. Montgomery, Jr., J. E. Peralta, F. Ogliaro, M. J. Bearpark, J. J. Heyd, E. N. Brothers, K. N. Kudin, V. N. Staroverov, T. A. Keith, R. Kobayashi, J. Normand, K. Raghavachari, A. P. Rendell, J. C. Burant, S. S. Iyengar, J. Tomasi, M. Cossi, J. M.

- Millam, M. Klene, C. Adamo, R. Cammi, J. W. Ochterski, R. L. Martin, K. Morokuma, O. Farkas, J. B. Foresman, and D. J. Fox, Gaussian, Gaussian 16, Revision A.03, Inc., Wallingford CT, 2016.
- [36] P. J. Hay, W. R. Wadt, *J. Chem. Phys.* 82(1), 299 (1985)

Figure 1. The structure of carbynes: (a) the schematic distribution of the electron density in cumulene and polyynes allotropes of carbyne. (b) shows the band structure of an infinite polyynes chain predicted by our ab-initio calculation, and the HOMO, LUMO doubly degenerate orbitals. (c) illustrates the concept of stabilisation of monoatomic carbon chains by gold nanoparticles in a solution. (d) shows schematically the energy level structure of a finite polyynes chain with two gold nanoparticles attached to its ends.

Figure 2. Optical investigation of carbyne chains in a colloidal solution: (a) the Raman spectra of the solution containing linear carbon chains stabilised by gold NPs. The peaks correspond to characteristic vibron modes of the polyynes allotrope. (b) the absorption spectrum (A (a.u.)) of the solution containing gold-stabilised carbon chains. The inset shows the decomposition of the experimental spectrum into a sequence of calculated absorption peaks corresponding to the polyynes chains of different lengths. (c) shows the absorption magnitude (marked as the A magnitude) distribution in straight polyynes chains extracted from the fit of the absorption spectra.

Deposition and characterisation of carbon chains: (a) illustrates the applied method of deposition of the aligned carbon chains stabilised by gold NPs of different sizes. Due to the difference in work functions of gold nanoparticles attached to the ends of the chain, it becomes dipole polarised. The external electric field orients the polarised chains, so that their majority appears to be aligned when deposited on a substrate by sputtering,

(b) shows the HR TEM profile of this structure measured in the direction perpendicular to the chains. The profile is taken along the red arrow in the HR TEM image shown in

(c) .

Figure 4. PL spectra of the deposited polyynes chains of different lengths (the number of atoms in the chain is indicated on the top of the corresponding spectral resonance). (a) shows the spectra taken at temperatures from 90 to 50K (red curve corresponds to 90 K, yellow curve corresponds to 80K, green curve corresponds to 70K, teal curve corresponds to 60K, blue curve corresponds to 50K). The laser excitation wavelength is 390 nm with the intensity of 5 mW and the acquisition time of 10 s. (b) shows the PL spectra taken at 4K. Red, blue and black curves correspond to the excitation wavelengths of 390, 380 and 370 nm, respectively. The acquisition time is 40 s.

Figure 5. The time-resolved photoluminescence data: (a) and (c) show the TRPL data acquired at the room temperature and at 4K, respectively. The insets show the spectral bands that correspond to the TRPL curves of (a,c), respectively. The colors match.(b) shows the extracted decay times of the TRPL signal taken at room temperature and Helium temperature, respectively. Red and black points correspond to the deduced radiative decay time at the room temperature (red) and Helium temperature (black). The blue points show the non-radiative decay times, extracted from the room temperature TRPL curves (a).

Figure 6. The scheme of excitonic transitions in a monoatomic polyynes chain. (a)

The neutral exciton (X) is formed by even and odd edge states that originate from the HOMO-LUMO pair. (b,c) The trion transitions in charged chains, where the left-right symmetry is broken so that the optical transition occurs between either the original HOMO state and the spin polarised electron state localised at one of the edges (X-) or between the hole state localised at one of the edges and the original LUMO state (X+). (d) The enlarged PL spectrum of a characteristic triplet corresponding to the 14- atom chain that shows the relative oscillator strengths of exciton and trion transitions. Molecular orbitals and total electron density plots for a model system containing a polyynes chain composed of 14 carbon atoms capped with two gold nanoparticles (C14- Au13₂) for HOMO (e), LUMO (f). The total calculated electron density (g). Red and blue lobes correspond to positive and negative values, respectively.

Supplementary Material to Excitons in linear carbon chains

Stella Kutrovskaia^{1,2,3*}, Anton Osipov^{3,4}, Stepan Baryshev⁵,
Anton Zasedatelev⁵, Alexey Povolotskiy⁶, Vlad Samyshkin³,
Olivia Pulci⁷, Davide Grassano⁷, Lorenzo Gontrani⁷, Richard
Hartmann⁸, Mikhail E. Portnoi^{9,10}, Alexey Kucherik^{1,2,3}, Pavlos
Lagoudakis^{5,11} and Alexey Kavokin^{1,2,11,12}

¹ School of Science, Westlake University, 18 Shilongshan Road, Hangzhou 310024, Zhejiang Province, China

² Institute of Natural Sciences, Westlake Institute for Advanced Study, 18 Shilongshan Road, Hangzhou 310024, Zhejiang Province, China

³ Department of Physics and Applied Mathematics, Stoletov Vladimir State University, 600000 Gorkii street, Vladimir, Russia

⁴ ILIT RAS — Branch of FSRC “Crystallography and Photonics” RAS, 1 Svyatoozerskaya, Shatura, 140700, Moscow region, Russia

⁵ Skolkovo Institute of Science and Technology, 30 Bolshoy Boulevard, bld. 1, 121205 Moscow, Russia

⁶ Institute of Chemistry, St. Petersburg State University, 198504, Ulianovskaya str. 5, St. Petersburg, Russia

⁷ Department of Physics, University of Rome Tor Vergata, Via della Ricerca Scientifica 1, I-00133 Rome, Italy

⁸ Physics Department, De La Salle University, 2401 Taft Avenue, 0922 Manila, Philippines

⁹ Physics and Astronomy, University of Exeter, Stocker Road, Exeter EX4 4QL, United Kingdom

¹⁰ ITMO University, St. Petersburg 197101, Russia

¹¹ Physics and Astronomy, University of Southampton, Highfield, Southampton, SO171BJ, United Kingdom

¹² Spin Optics Laboratory, St. Petersburg State University, 198504, Ulianovskaya str. 1, St. Petersburg, Russia

September 2019

E-mail: stella.kutrovskaia@westlake.edu.cn

1. The ab-initio calculation results for a non-stabilised carbon chain

The Density Functional Theory calculations for the carbon chain non stabilised with gold (H-terminated) were performed using the Gaussian 16 package, employing the PBE0 kernel with triple-zeta 6-311+G(d,p) basis set. In the geometry-optimised chain (in polyene configuration) one can see that HOMO and LUMO electron densities are spread over the whole chain in the absence of gold anchors at the ends.

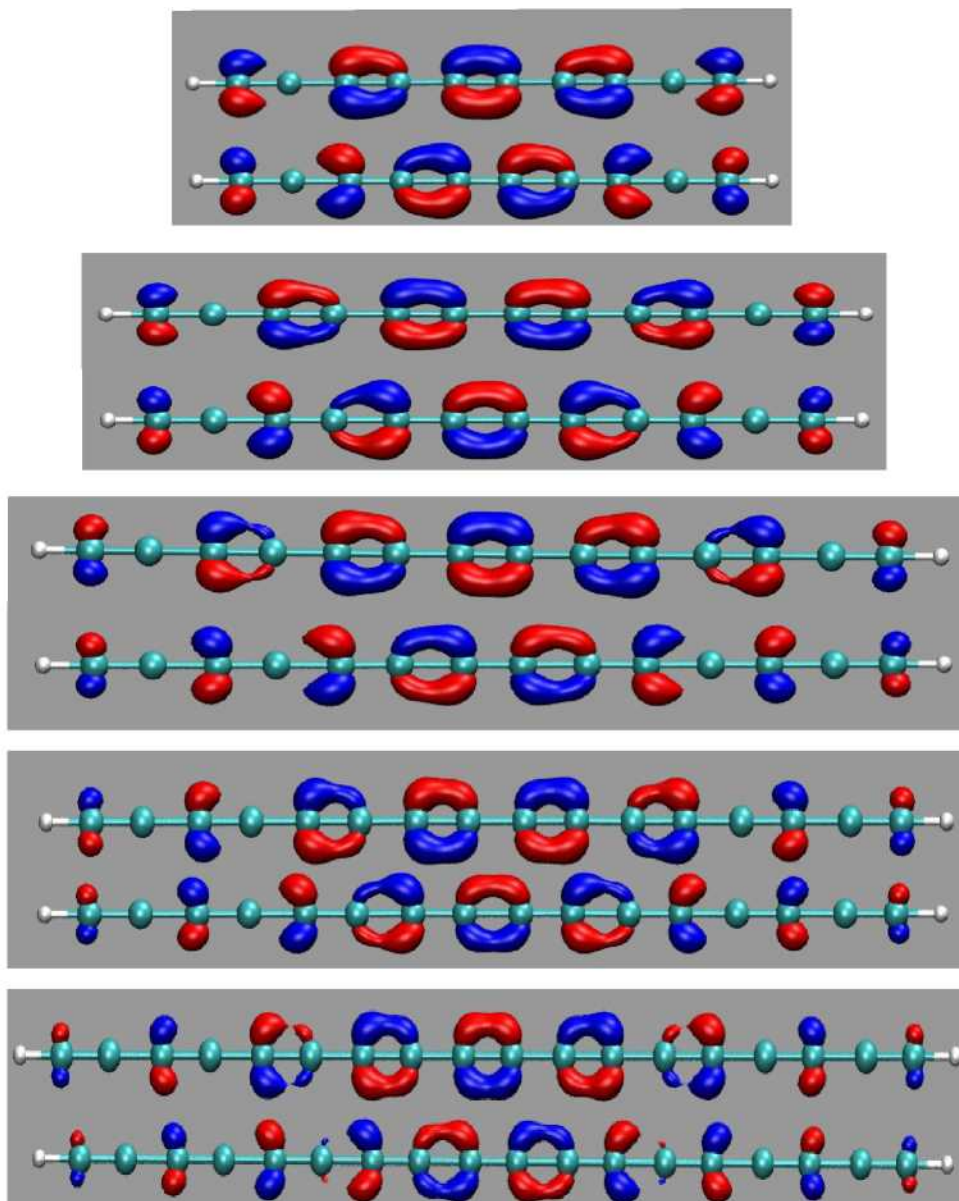


Figure S1: Molecular orbitals for C10, C12, C14, C16, C18 polyynes fragments. Top row: HOMO; Bottom row; LUMO. Red and blue lobes correspond to positive and negative values, respectively.

Supplementary Material to Excitons in linear carbon chains

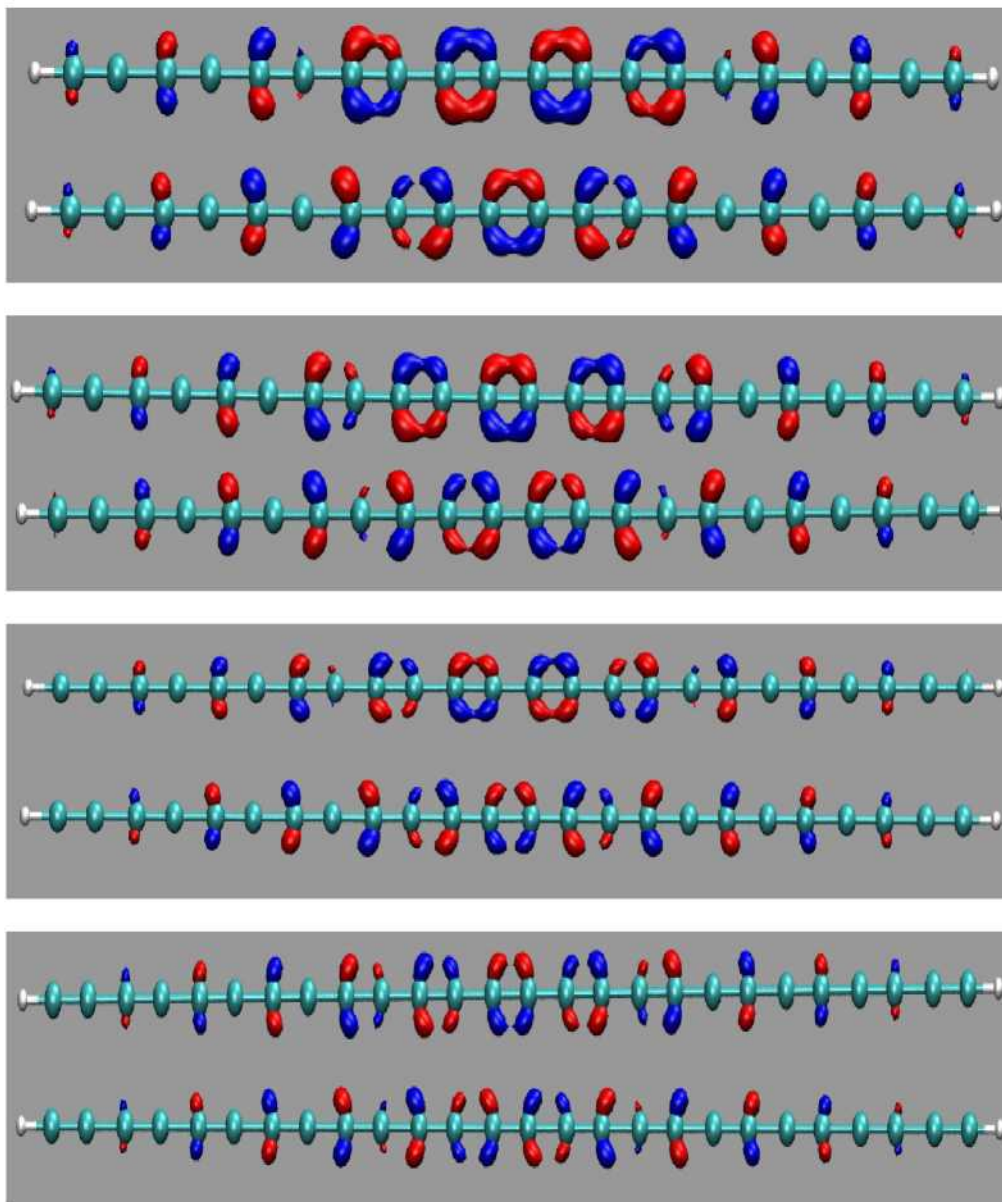


Figure S2: Molecular orbitals for C₂₀, C₂₂, C₂₄ and C₂₆ polyynes fragments. Top row: HOMO; Bottom row; LUMO. Red and blue lobes correspond to positive and negative values, respectively.